International Journal of Engineering Science 148 (2020) 103210

Contents lists available at ScienceDirect

International Journal of Engineering Science

journal homepage: www.elsevier.com/locate/ijengsci

Torsional stability capacity of a nano-composite shell based on a nonlocal strain gradient shell model under a three-dimensional magnetic field ☆

Mohammad Malikan [a], Maxim Krasheninnikov [b], Victor A. Eremeyev [a,b,*]

[a] Department of Mechanics of Materials and Structures, Faculty of Civil and Environmental Engineering, Gdansk University of Technology, 80-233 Gdansk, Poland

[b] R. E. Alekseev Nizhny Novgorod Technical University, Minin St., 24, Nizhny Novgorod, 603950 Russia

ARTICLE INFO

Article history:
Received 19 December 2019
Accepted 25 December 2019
Available online xxx

Keywords:
Single-walled composite nano-shell
Torsional buckling
Three-dimensional magnetic field
Nonlocal strain gradient shell model
Analytical solution

ABSTRACT

This paper considers a single-walled composite nano-shell (SWCNS) exposed in a torsional critical stability situation. As the magnetic field affects remarkably nanostructures in the small size, a three-dimensional magnetic field is assessed which contains magnetic effects along the circumferential, radial and axial coordinates system. Based on the results of the nonlocal model of strain gradient small-scale approach and the first-order shear deformation shell theory (FSDST), the problem is estimated. Afterward, the numerical results are taken analytically and compared with other existing literature. Hereafter, the influences of various factors, such as the magnetic field, are discussed deeply. It is observed that when the magnetic field is studied in three dimensions, the transverse magnetic effect is the most serious factor that affects fundamentally the torsional stability of the shell.

1. Introduction

Due to the urgent need of industries for high strength structures with low weight, nano-composite shells are a good choice for this field. Over the years, nano-composite materials have been found from laboratory to commercial and industrial applications and have also many applications in various industries such as aerospace, defense, offshore and automotive. Some nano-composite structures which have been made, e.g. magnetic nano-composite structures, have received further attention over the previous years. These materials present impressive properties that outweigh the properties of conventional composite materials. The magnetic nano-composite structures are useful for producers of actuators and small motors, especially computer hardware, audio and video (Elimelech, Gregory, Jia & Williams, 1995).

To design different structures, analyzes such as static, dynamic, vibrational, fracture and buckling ones are performed. Since cylindrical nano-shell/tube structures are more susceptible to buckling loads, stability analysis is one of the most

☆ Preprint submitted to International Journal of Engineering Science December 19, 2019

* Corresponding author at: Department of Mechanics of Materials and Structures, Faculty of Civil and Environmental Engineering, Gdansk University of Technology, 80-233 Gdansk, Poland.

E-mail addresses: mohammad.malikan@pg.edu.pl (M. Malikan), maxim.krasheninnikov@mail.ru (M. Krasheninnikov), victor.eremeev@pg.edu.pl (V.A. Eremeyev).

https://doi.org/10.1016/j.ijengsci.2019.103210

serious analyses of these types of structures. Among the nano-shell structures, the carbon nanotubes (CNTs) are the most customary nano-shells that have been greatly investigated. Han and Lu (2003) based on the local continuum mechanics, studied the torsional stability of a double-walled carbon nanotube (DWCNT) based on considering an elastic substrate. They employed the classical shell model and solved the gained equations by means of the Navier solution technique. Wang, Yang and Dong (2005) considered multi-walled carbon nanotubes (MWCNTs) under a torsional stability condition based on the local classical continuum shell model. Lu and Wang (2006) combined torsional and axial stability conditions in order to estimate the local continuum shell MWCNTs. Zhang and Shen (2006) examined a single-walled carbon nanotube (SWCNT) with the help of molecular dynamics (MD) simulation subjected to torsion, axial and external pressures by assuming a thermal surrounding. In some valuable research works, other researchers have also studied CNTs in the case of torsional stability (Jeong, Lim & Sinnott, 2007; Wang, Quek & Varadan, 2007; Yang & Wang, 2007; Zhang & Wang, 2008). Later, Shen and Zhang (2010) modeled a DWCNT by using first-order shear deformation shell theory (FSDST) and in conjunction with nonlocal elasticity and also considering the thermal environment. Hao, Guo and Wang (2010), Natsuki, Tsuchiya, Ni and Endo (2010), on the other hand, worked on the shell model of DWCNTs based on the nonlocal elasticity theory. Khademolhosseini, Rajapakse and Nojeh (2010) used a modified Timoshenko shell model to evaluate a SWCNT in a shell domain based on the nonlocal theory of Eringen. In various conditions and cases, some other studies have been done on the CNTs exposed to torsional stability (Chowdhurry, Wang & Koh, 2014; Parvaneh, Shariati, Torabi, Masood & Sabeti, 2012; Song & Zha, 2011; Zhang & Li, 2015). More newly, Xiaohu, Yugang and Hanzhou (2013) carried out an electric and thermal field around the CNTs exposed to torsion by examining size effects. Ghorbanpour Arani, Abdollahian, Kolahchi and Rahmati (2013) analyzed a DWCNT subjected to the torsional critical force and thermal effects with considering piezoelectricity impact. They applied the FSDST and also assumed a matrix outer the system. The piezoelectric field was assumed in one direction. They solved the harvested stability relations regarding the Navier approach. In an effective paper, Mehralian, Tadi Beni and Karimi Zeverdejani (2017) simulated natural frequencies of a shell FSDST-CNTs by using MD based on different small-scale theories, namely modified couple stress theory (CST), nonlocal elasticity theory (NT), strain gradient theory (ST) and nonlocal strain gradient theory (NSGT). Their numerical outcomes approved more conformity of the results of nonlocal strain gradient theory with MD. More recently, however, Shojaeefard, Mahinzare, Safarpour, Saeidi Googarchin and Ghadiri (2018) presented the natural frequencies of a Timoshenko nano-composite shell by taking electric-magnetic and thermal environments into account. They assumed that the shell was under an ultra-fast rotation and was inserted in an elastic substrate. To capture the small-scale effects, the modified couple stress theory was discussed. Finally, they calculated the natural frequencies of the shell in the mentioned conditions based on the Navier analytical method and also generalized differential quadrature (GDQ) numerical method. Sahmani and Aghdam (2018) established the nonlocal strain gradient approach to study axial stability and post-stability responses of a nano-shell incorporating electric and magnetic field effects. They used the classical shell model in employing the cartesian coordinate system. To give their results numerically, they applied an improved perturbation technique.

Until the date, no paper has been recorded on an analysis of the torsional stability of nano-composite shells regarding a three-dimensional magnetic field based on the NSGT. Therefore, this paper studies a nano-composite material, i.e. $BaTiO_3$-$CoFe_2O_3$ in a shell-like structure. As this material is a smart piezomagnetic structure, it could be utilized in several nano-electro/magneto-mechanical systems. Hence, torsional stability analysis of such the nanostructure can be significant resulting in many advantages. This motivated authors to assess the torsional stability of the nano-composite shell while the magnetic field has three-dimensional influences. To predict the motion of the model's nodes, the first-order shear deformation shell hypothesis is employed. To address the size effects, the nonlocal theory of strain gradient is practiced. To attain the graphs based on the numerical outcomes, an analytical solution technique is exploited. In the results section, different key factors, such as the magnetic field and small-scale act, are taken into the investigation.

2. Basic formulation

A schematic picture of the SWCNS is below presented in which the radius, length, and thickness of the model are respectively, *R, L*, and *h* Figure 1.

In this research, concerning the cylindrical shape of the nano-shell, the first-order shear deformation shell theory (FSDST) is given by Ghorbanpour Arani et al. (2013), Mehralian et al. (2017), Shojaeefard et al. (2018)

$$\begin{Bmatrix} u_1(x,\theta,z) \\ u_2(x,\theta,z) \\ u_3(x,\theta,z) \end{Bmatrix} = \begin{Bmatrix} u(x,\theta)+z\varphi_x(x,\theta) \\ v(x,\theta)+z\varphi_\theta(x,\theta) \\ w(x,\theta) \end{Bmatrix} \tag{1}$$

in which $u_i(i=1,2,3)$ represents the displacement components of each point of the nano-shell along axial, circumferential and radial axes, respectively, $u(x,\theta)$, $v(x,\theta)$ and $w(x,\theta)$ correspond to the mid-plan displacements along with axial, circumferential and radial directions, φ_x and φ_θ display the rotation around the axial and circumferential axes. Furthermore, a coordinate for the thickness of the nano-shell is chosen as *z*.

Based on the Lagrangian strain, a continuum nonlinear strain-displacement equation can be written as

$$\{\varepsilon_{ij}\} = \frac{1}{2}\left\{\frac{\partial u_i}{\partial x_j}+\frac{\partial u_j}{\partial x_i}+\frac{\partial u_k}{\partial x_i}\frac{\partial u_k}{\partial x_j}\right\} \tag{2}$$

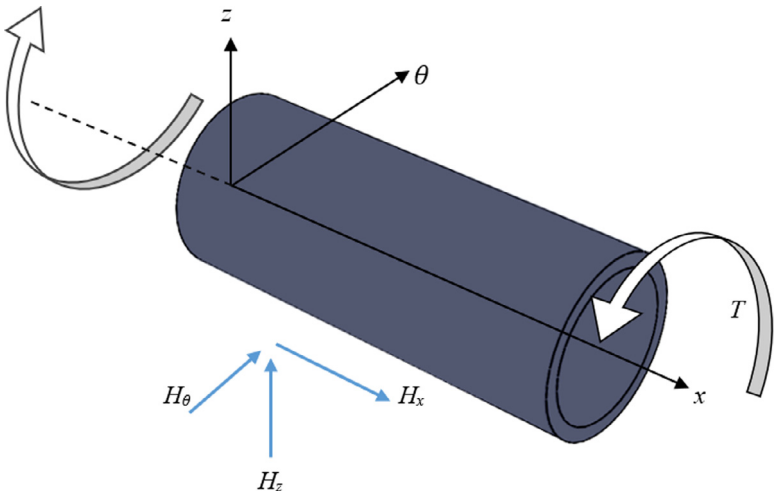

Fig. 1. A SWCNS under a three-dimensional magnetic field exposed to the torsional force.

Regarding the principle of curvilinear derivation and also the model of cylindrical shell, the components of strain for the shell SWCNS based on the Eq. (2) can be expanded as below

$$\begin{Bmatrix} \varepsilon_{xx} \\ \varepsilon_{\theta\theta} \\ \gamma_{xz} \\ \gamma_{x\theta} \\ \gamma_{\theta z} \end{Bmatrix} = \begin{Bmatrix} \frac{\partial u}{\partial x} + z\frac{\partial \varphi_x}{\partial x} + \frac{1}{2}\left(\frac{\partial w}{\partial x}\right)^2 \\ \frac{1}{R}\left(w + \frac{\partial v}{\partial \theta}\right) + \frac{1}{2R^2}\left(\frac{\partial w}{\partial \theta}\right)^2 + \frac{z}{R}\frac{\partial \varphi_\theta}{\partial \theta} \\ \varphi_x + \frac{\partial w}{\partial x} \\ \frac{\partial v}{\partial x} + \frac{1}{R}\left(\frac{\partial u}{\partial \theta} + \frac{\partial w}{\partial \theta}\frac{\partial w}{\partial x}\right) + z\left(\frac{\partial \varphi_\theta}{\partial x} + \frac{1}{R}\frac{\partial \varphi_x}{\partial \theta}\right) \\ \frac{1}{R}\left(\frac{\partial w}{\partial \theta} - v\right) + \varphi_\theta \end{Bmatrix} \tag{3}$$

The tensor of classical stresses of an element of the nano-shell along axial, circumferential and radial directions that includes the terms of magnetic and mechanic can be written as (Ghorbanpour Arani et al., 2013; Mehralian et al., 2017; Shojaeefard et al., 2018)

$$\begin{Bmatrix} \sigma_{xx} \\ \sigma_{\theta\theta} \\ \tau_{x\theta} \\ \tau_{xz} \\ \tau_{\theta z} \end{Bmatrix} = \begin{bmatrix} \overline{C}_{11} & \overline{C}_{12} & 0 & 0 & 0 \\ \overline{C}_{12} & \overline{C}_{22} & 0 & 0 & 0 \\ 0 & 0 & \overline{C}_{44} & 0 & 0 \\ 0 & 0 & 0 & \overline{C}_{55} & 0 \\ 0 & 0 & 0 & 0 & \overline{C}_{66} \end{bmatrix} \begin{Bmatrix} \varepsilon_{xx} \\ \varepsilon_{\theta\theta} \\ \gamma_{x\theta} \\ \gamma_{xz} \\ \gamma_{\theta z} \end{Bmatrix} - \begin{bmatrix} 0 & 0 & \overline{q}_{31} \\ 0 & 0 & \overline{q}_{32} \\ 0 & 0 & 0 \\ \overline{q}_{15} & 0 & 0 \\ 0 & \overline{q}_{24} & 0 \end{bmatrix} \begin{Bmatrix} \overline{H}_x \\ \overline{H}_\theta \\ \overline{H}_z \end{Bmatrix} \tag{4}$$

where the H_k is the magnetic field. Moreover, $\overline{q}_{ij}$ depicts piezomagnetic moduli related to the magnetic property of the nano-shell. Also, σ_{ij} and ε_{ij} are respectively the static stress and strain fields. Additionally, $C_{ijkl}(i, j = 1, ..., 6)$ is the stiffness matrix defined as follows

$$\begin{Bmatrix} \overline{C}_{11} \\ \overline{C}_{12} \\ \overline{C}_{22} \\ \overline{C}_{44} \\ \overline{C}_{55} \\ \overline{C}_{66} \end{Bmatrix} = \begin{Bmatrix} C_{11} - \frac{C_{13}^2}{C_{33}} \\ C_{12} - \frac{C_{13}C_{23}}{C_{33}} \\ C_{22} - \frac{C_{23}^2}{C_{33}} \\ C_{44} \\ C_{55} \\ C_{66} \end{Bmatrix} \tag{5}$$

The Hamilton's principle is utilized to derive the equilibrium equations as (Mikhasev, Eremeyev, Wilde & Maevskaya, 2019)

$$\delta\Pi = \int_{t_1}^{t_2} (\delta K - (\delta U - \delta W))dt = 0 \tag{6}$$

in which the variated kinetic and strain energies are respectively δK and δU. On the other hand, the work of outer loads is δW. Note that, in this paper, the effects of mass moment of inertia are removed.

The variated strain energy is presented below

$$\delta U = \iiint_v \left(\sigma_{ij}\delta\varepsilon_{ij} - B_k\delta H_k\right)dV = 0 \tag{7}$$

where the B_k is the magnetic induction which can be formulated as follows

$$\begin{Bmatrix} \overline{B}_x \\ \overline{B}_\theta \\ \overline{B}_z \end{Bmatrix} = \begin{bmatrix} 0 & 0 & 0 & \overline{q}_{15} & 0 \\ 0 & 0 & 0 & 0 & \overline{q}_{24} \\ \overline{q}_{31} & \overline{q}_{32} & 0 & 0 & 0 \end{bmatrix} \begin{Bmatrix} \varepsilon_{xx} \\ \varepsilon_{\theta\theta} \\ \gamma_{x\theta} \\ \gamma_{xz} \\ \gamma_{\theta z} \end{Bmatrix} + \begin{bmatrix} \overline{\eta}_{11} & 0 & 0 \\ 0 & \overline{\eta}_{22} & 0 \\ 0 & 0 & \overline{\eta}_{33} \end{bmatrix} \begin{Bmatrix} \overline{H}_x \\ \overline{H}_\theta \\ \overline{H}_z \end{Bmatrix} \tag{8}$$

in which $\overline{\eta}_{ij}$ shows a magnetic quantity. The magnetic constants can be expressed as

$$\begin{Bmatrix} \overline{q}_{31} \\ \overline{q}_{32} \\ \overline{q}_{15} \\ \overline{q}_{24} \end{Bmatrix} = \begin{Bmatrix} q_{31} - \frac{C_{13}q_{33}}{C_{33}} \\ q_{32} - \frac{C_{23}q_{33}}{C_{33}} \\ q_{15} \\ q_{24} \end{Bmatrix}; \begin{Bmatrix} \overline{\eta}_{11} \\ \overline{\eta}_{22} \\ \overline{\eta}_{33} \end{Bmatrix} = \begin{Bmatrix} \eta_{11} \\ \eta_{22} \\ \eta_{33} + \frac{q_{33}^2}{C_{33}} \end{Bmatrix} \tag{9}$$

Based on the available magnetic potential, the following linear function can be employed (Ghorbanpour Arani et al., 2013; Mehralian et al., 2017; Shojaeefard et al., 2018)

$$\overline{\Psi}(x,\theta,z) = -\cos\left(\frac{\pi z}{h}\right)\Psi(x,\theta) + \frac{2z\psi_0}{h} \tag{10}$$

in which the initial magnetic potential is symbolized with Ψ(x, y), and the magnetic potential is ψ_0.

By means of Eq. (10), the magnetic field can be indicated in three dimensions as below

$$\begin{Bmatrix} \overline{H}_x \\ \overline{H}_\theta \\ \overline{H}_z \end{Bmatrix} = \begin{Bmatrix} -\frac{\partial\overline{\Psi}}{\partial x} \\ -\frac{1}{R+z}\frac{\partial\overline{\Psi}}{\partial\theta} \\ -\frac{\partial\overline{\Psi}}{\partial z} \end{Bmatrix} = \begin{Bmatrix} \cos\left(\frac{\pi z}{h}\right)\frac{\partial\Psi}{\partial x} \\ \frac{1}{R+z}\cos\left(\frac{\pi z}{h}\right)\frac{\partial\Psi}{\partial\theta} \\ -\frac{\pi}{h}\sin\left(\frac{\pi z}{h}\right)\Psi - \frac{2\psi_0}{h} \end{Bmatrix} \tag{11}$$

Assuming an element of the nano-shell in an equilibrium condition gives us the stress resultants as

$$\{N_{xx}, N_{\theta\theta}, N_{x\theta}, M_{xx}, M_{x\theta}, M_{\theta\theta}, Q_{xz}, Q_{\theta z}\} = \int_{-0.5h}^{0.5h} \{\sigma_{xx}, \sigma_{\theta\theta}, \sigma_{x\theta}, \sigma_{xx}z, \sigma_{x\theta}z, \sigma_{\theta\theta}z, k\tau_{xz}, k\tau_{\theta z}\}dz \tag{12}$$

where the moment stress resultants (M_{xx}, $M_{x\theta}$, $M_{\theta\theta}$), the transverse shear stress resultants (Q_{xz}, $Q_{\theta z}$), and the axial stress resultants (N_{xx}, $N_{\theta\theta}$, $N_{x\theta}$) are shown. In addition, k defines a shear correction factor by which the value of the transverse shear stress along the thickness of the model can be refined.

Hence, based on Eq. (4), Eq. (12) can be developed as below

$$\begin{Bmatrix} \mathrm{N_{xx}} \\ \mathrm{N_{\theta\theta}} \\ \mathrm{N_{x\theta}} \\ \mathrm{M_{xx}} \\ \mathrm{M_{\theta\theta}} \\ \mathrm{M_{x\theta}} \\ \mathrm{Q_{xz}} \\ \mathrm{Q_{\theta z}} \end{Bmatrix} = \begin{bmatrix} \mathrm{A_{11}} & \mathrm{A_{12}} & 0 & 0 & 0 & 0 & 0 & 0 \\ \mathrm{A_{21}} & \mathrm{A_{22}} & 0 & 0 & 0 & 0 & 0 & 0 \\ 0 & 0 & \mathrm{A_{44}} & 0 & 0 & 0 & 0 & 0 \\ 0 & 0 & 0 & \mathrm{D_{11}} & \mathrm{D_{12}} & 0 & 0 & 0 \\ 0 & 0 & 0 & \mathrm{D_{21}} & \mathrm{D_{22}} & 0 & 0 & 0 \\ 0 & 0 & 0 & 0 & 0 & \mathrm{D_{66}} & 0 & 0 \\ 0 & 0 & 0 & 0 & 0 & 0 & kA_{55} & 0 \\ 0 & 0 & 0 & 0 & 0 & 0 & 0 & kA_{66} \end{bmatrix} \times \begin{Bmatrix} \frac{\partial u}{\partial x} + \frac{1}{2}\left(\frac{\partial w}{\partial x}\right)^2 \\ \frac{1}{R}\left(w + \frac{\partial v}{\partial\theta}\right) + \frac{1}{2R^2}\left(\frac{\partial w}{\partial\theta}\right)^2 \\ \frac{\partial v}{\partial x} + \frac{1}{R}\left(\frac{\partial u}{\partial\theta} + \frac{\partial w}{\partial\theta}\frac{\partial w}{\partial x}\right) \\ \frac{\partial\varphi_x}{\partial x} \\ \frac{1}{R}\frac{\partial\varphi_\theta}{\partial\theta} \\ \frac{\partial\varphi_\theta}{\partial x} + \frac{1}{R}\frac{\partial\varphi_x}{\partial\theta} \\ \varphi_x + \frac{\partial w}{\partial x} \\ \frac{1}{R}\left(\frac{\partial w}{\partial\theta} - v\right) + \varphi_\theta \end{Bmatrix} + \begin{Bmatrix} 2\bar{q}_{31}\psi_0 \\ 2\bar{q}_{32}\psi_0 \\ 0 \\ X_{35}\Psi \\ X_{63}\Psi \\ 0 \\ -X_{21}\frac{\partial\Psi}{\partial x} \\ -X_{23}\frac{\partial\Psi}{\partial\theta} \end{Bmatrix} \tag{13}$$

in which

$$A_{ij} = \int_{-\frac{h}{2}}^{\frac{h}{2}} \bar{\mathrm{C}}_{\mathrm{ij}}dz{:}(i,j=1,2,4,6), D_{ij} = \int_{-\frac{h}{2}}^{\frac{h}{2}} \bar{\mathrm{C}}_{\mathrm{ij}}z^2dz{:}(i,j=1,2,6) \tag{14}$$

By doing $\delta\Pi$i=0, the equilibrium equations can be obtained as

$$\delta u_1 = 0 : \frac{\partial N_{xx}}{\partial x} + \frac{1}{R}\frac{\partial N_{x\theta}}{\partial\theta} = 0 \tag{15a}$$

$$\delta u_2 = 0 : \frac{1}{R}\frac{\partial N_{\theta\theta}}{\partial\theta} + \frac{\partial N_{x\theta}}{\partial x} + \frac{Q_{\theta z}}{R} = 0 \tag{15b}$$

$$\delta u_3 = 0 : \frac{\partial}{\partial x}\left(N_{xx}\frac{\partial w}{\partial x}\right) + \frac{1}{R}\frac{\partial}{\partial\theta}\left(N_{\theta\theta}\frac{1}{R}\frac{\partial w}{\partial\theta}\right) + \frac{1}{R}\frac{\partial}{\partial\theta}\left(N_{x\theta}\frac{\partial w}{\partial x}\right) + \frac{1}{R}\frac{\partial}{\partial x}\left(N_{x\theta}\frac{\partial w}{\partial\theta}\right)$$

$$-\frac{N_{\theta\theta}}{R}+\frac{\partial Q_{xz}}{\partial x}+\frac{1}{R}\frac{\partial Q_{\theta z}}{\partial \theta}=0 \tag{15c}$$

$$\delta\varphi_x=0:\frac{\partial M_{xx}}{\partial x}+\frac{1}{R}\frac{\partial M_{x\theta}}{\partial \theta}-Q_{xz}=0 \tag{15d}$$

$$\delta\varphi_\theta=0:\frac{1}{R}\frac{\partial M_{\theta\theta}}{\partial \theta}+\frac{\partial M_{x\theta}}{\partial x}-Q_{\theta z}=0 \tag{15e}$$

$$\delta\Psi=0;\int_{-h/2}^{h/2}\left[\frac{\partial \bar{B}_x}{\partial x}\cos\left(\frac{\pi z}{h}\right)+\frac{1}{R+z}\frac{\partial \bar{B}_\theta}{\partial \theta}\cos\left(\frac{\pi z}{h}\right)+\frac{\pi}{h}\bar{B}_z\sin\left(\frac{\pi z}{h}\right)\right]dz=0 \tag{15f}$$

where

$$\begin{Bmatrix}\bar{B}_x\\ \bar{B}_\theta\\ \bar{B}_z\end{Bmatrix}=\int_{-h/2}^{h/2}\begin{Bmatrix}B_x\cos\left(\frac{\pi z}{h}\right)\\ B_\theta\frac{1}{R+z}\cos\left(\frac{\pi z}{h}\right)\\ B_z\frac{\pi}{h}\sin\left(\frac{\pi z}{h}\right)\end{Bmatrix}dz=\begin{Bmatrix}X_{21}\left(\varphi_x+\frac{\partial w}{\partial x}\right)+Y_{11}\frac{\partial \Psi}{\partial x}\\ X_{23}\left(\frac{1}{R}\left(\frac{\partial w}{\partial \theta}-v\right)+\varphi_\theta\right)+Y_{22}\frac{\partial \Psi}{\partial \theta}\\ X_{34}\frac{\partial u}{\partial x}+X_{35}\frac{\partial \varphi_x}{\partial x}+X_{63}\frac{1}{R}\left(\frac{\partial v}{\partial \theta}+w\right)+X_{64}\frac{1}{R}\frac{\partial \varphi_\theta}{\partial \theta}-Y_{33}\Psi\end{Bmatrix} \tag{16}$$

The additional parameters in Eqs. (13) and (16) are

$$\begin{Bmatrix}X_{21}\\ X_{23}\\ X_{34}\\ X_{35}\\ X_{63}\\ X_{64}\end{Bmatrix}=\int_{-h/2}^{h/2}\begin{Bmatrix}\bar{q}_{15}\cos\left(\frac{\pi}{h}z\right)\\ \bar{q}_{24}\frac{1}{R+z}\cos\left(\frac{\pi}{h}z\right)\\ \bar{q}_{31}\frac{\pi}{h}\sin\left(\frac{\pi}{h}z\right)\\ \bar{q}_{31}\frac{\pi}{h}z\sin\left(\frac{\pi}{h}z\right)\\ \bar{q}_{32}\frac{\pi}{h}\sin\left(\frac{\pi}{h}z\right)\\ \bar{q}_{32}\frac{\pi}{h}z\sin\left(\frac{\pi}{h}z\right)\end{Bmatrix}dz;\begin{Bmatrix}Y_{11}\\ Y_{22}\\ Y_{33}\end{Bmatrix}=\int_{-h/2}^{h/2}\begin{Bmatrix}\bar{\eta}_{11}\cos^2\left(\frac{\pi}{h}z\right)\\ \bar{\eta}_{22}\left(\frac{1}{R+z}\right)^2\cos^2\left(\frac{\pi}{h}z\right)\\ \bar{\eta}_{33}\left(\frac{\pi}{h}\right)^2\sin^2\left(\frac{\pi}{h}z\right)\end{Bmatrix}dz \tag{17}$$

Following on from the application of small-scale theories, such as (Eringen, 1983; Farajpour, Ghayesh & Farokhi, 2019; Mikhasev & Nobili, 2019; Reddy, 2007), couple stress (Akbarzadeh Khorshidi, 2018; Akgöz & Civalek, 2012; Malikan, 2017) and the strain gradient (Gholami, Darvizeh, Ansari & Sadeghi, 2016; Lurie & Solyaev, 2019a; Lurie and Solyaev, 2019b; Solyaev, Lurie, Koshurina, Dobryanskiy & Kachanov, 2019; Solyaev & Lurie, 2019), a new theory has been proposed (Lim, Zhang & Reddy, 2015) that presents two different properties of nanomaterials (stiffness-hardening and stiffness-softening), namely nonlocal theory of strain gradient with which much research works have been demonstrated (Arefi, Kiani & Rabczuk, 2019; Karami, Shahsavari & Janghorban, 2019; Malikan & Nguyen, 2018; Malikan, Dimitri & Tornabene, 2019; Sahmani & Aghdam, 2017; She, Yuan, Karami, Ren & Xiao, 2019). This theory in its differential form is formulated as

$$\left(1-\mu\nabla^2\right)\sigma_{ij}=\mathrm{C}_{ijkl}\left(1-l^2\nabla^2\right)\varepsilon_{kl} \tag{18}$$

in which the $\nabla^2=\frac{\partial^2}{\partial x^2}+\frac{1}{R^2}\frac{\partial^2}{\partial \theta^2}$ is the Laplace operator in cylindrical coordinates, l, and μ exhibit the small scale parameters which respectively define two independent effects for nanostructures. The first one assigns hardening effect resulted from reducing the size from macro to nano and the second one defines the interaction between atoms in an atomic lattice which means stress nonlocality.

According to Eq. (18), Eq. (13) in the NSGT form becomes

$$\left[N_{xx}-\mu\left(\frac{\partial^2 N_{xx}}{\partial x^2}+\frac{1}{R^2}\frac{\partial^2 N_{xx}}{\partial \theta^2}\right)\right]=\left(1-l^2\nabla^2\right)\left\{\mathrm{A}_{11}\left[\frac{\partial u}{\partial x}+\frac{1}{2}\left(\frac{\partial w}{\partial x}\right)^2\right]+\mathrm{A}_{12}\left[\frac{1}{R}\left(w+\frac{\partial v}{\partial \theta}\right)+\frac{1}{2R^2}\left(\frac{\partial w}{\partial \theta}\right)^2\right]\right\}+2\bar{q}_{31}\psi_0 \tag{19a}$$

$$\left[N_{\theta\theta}-\mu\left(\frac{\partial^2 N_{\theta\theta}}{\partial x^2}+\frac{1}{R^2}\frac{\partial^2 N_{\theta\theta}}{\partial \theta^2}\right)\right]=\left(1-l^2\nabla^2\right)\left\{\mathrm{A}_{21}\left[\frac{\partial u}{\partial x}+\frac{1}{2}\left(\frac{\partial w}{\partial x}\right)^2\right]+\mathrm{A}_{22}\left[\frac{1}{R}\left(w+\frac{\partial v}{\partial \theta}\right)+\frac{1}{2R^2}\left(\frac{\partial w}{\partial \theta}\right)^2\right]\right\}+2\bar{q}_{32}\psi_0 \tag{19b}$$

$$\left[N_{x\theta}-\mu\left(\frac{\partial^2 N_{x\theta}}{\partial x^2}+\frac{1}{R^2}\frac{\partial^2 N_{x\theta}}{\partial \theta^2}\right)\right]=\mathrm{A}_{44}\left(1-l^2\nabla^2\right)\left[\frac{\partial v}{\partial x}+\frac{1}{R}\left(\frac{\partial u}{\partial \theta}+\frac{\partial w}{\partial \theta}\frac{\partial w}{\partial x}\right)\right] \tag{19c}$$

$$\left[M_{xx}-\mu\left(\frac{\partial^2 M_{xx}}{\partial x^2}+\frac{1}{R^2}\frac{\partial^2 M_{xx}}{\partial\theta^2}\right)\right]=\left(1-l^2\nabla^2\right)\left(\mathrm{D}_{11}\frac{\partial\varphi_x}{\partial x}+\mathrm{D}_{12}\frac{1}{R}\frac{\partial\varphi_\theta}{\partial\theta}\right)+X_{35}\Psi \tag{19d}$$

$$\left[M_{\theta\theta}-\mu\left(\frac{\partial^2 M_{\theta\theta}}{\partial x^2}+\frac{1}{R^2}\frac{\partial^2 M_{\theta\theta}}{\partial\theta^2}\right)\right]=\left(1-l^2\nabla^2\right)\left(\mathrm{D}_{21}\frac{\partial\varphi_x}{\partial x}+\mathrm{D}_{22}\frac{1}{R}\frac{\partial\varphi_\theta}{\partial\theta}\right)+X_{63}\Psi \tag{19e}$$

$$\left[M_{x\theta}-\mu\left(\frac{\partial^2 M_{x\theta}}{\partial x^2}+\frac{1}{R^2}\frac{\partial^2 M_{x\theta}}{\partial\theta^2}\right)\right]=\mathrm{D}_{66}\left(1-l^2\nabla^2\right)\left(\frac{\partial\varphi_\theta}{\partial x}+\frac{1}{R}\frac{\partial\varphi_x}{\partial\theta}\right) \tag{19f}$$

$$\left[Q_{xz}-\mu\left(\frac{\partial^2 Q_{xz}}{\partial x^2}+\frac{1}{R^2}\frac{\partial^2 Q_{xz}}{\partial\theta^2}\right)\right]=A_{55}\left(1-l^2\nabla^2\right)\left(\varphi_x+\frac{\partial w}{\partial x}\right)-X_{21}\frac{\partial\Psi}{\partial x} \tag{19g}$$

$$\left[Q_{\theta z}-\mu\left(\frac{\partial^2 Q_{\theta z}}{\partial x^2}+\frac{1}{R^2}\frac{\partial^2 Q_{\theta z}}{\partial\theta^2}\right)\right]=A_{66}\left(1-l^2\nabla^2\right)\left(\frac{1}{R}\left(\frac{\partial w}{\partial\theta}-v\right)+\varphi_\theta\right)-X_{23}\frac{\partial\Psi}{\partial\theta} \tag{19h}$$

By substituting Eq. (19) into Eq. (15), and based on Eq. (13), and also by linearizing the obtained equations, we derive the stability equations as below

$$\left(1-l^2\nabla^2\right)\left\{\left[\mathrm{A}_{11}\frac{\partial^2 u}{\partial x^2}+\mathrm{A}_{12}\frac{1}{R}\left(\frac{\partial w}{\partial x}+\frac{\partial^2 v}{\partial x\partial\theta}\right)\right]+\mathrm{A}_{44}\frac{1}{R}\left(\frac{\partial^2 v}{\partial x\partial\theta}+\frac{1}{R}\frac{\partial^2 u}{\partial\theta^2}\right)\right\}=0 \tag{20a}$$

$$\left(1-l^2\nabla^2\right)\left\{\mathrm{A}_{44}\left(\frac{\partial^2 v}{\partial x^2}+\frac{1}{R}\frac{\partial^2 u}{\partial x\partial\theta}\right)+\left[\frac{\mathrm{A}_{21}}{R}\frac{\partial^2 u}{\partial x\partial\theta}+\frac{\mathrm{A}_{22}}{R^2}\left(\frac{\partial w}{\partial\theta}+\frac{\partial^2 v}{\partial\theta^2}\right)\right]+\frac{A_{66}}{R}\left[\frac{1}{R}\left(\frac{\partial w}{\partial\theta}-v\right)+\varphi_\theta\right]\right\}-\frac{X_{23}}{R}\frac{\partial\Psi}{\partial\theta}=0 \tag{20b}$$

$$\begin{aligned}&\left(1-\mu\nabla^2\right)\left(N^0_{xx}\frac{\partial^2 w}{\partial x^2}+\frac{2}{R}N^0_{x\theta}\frac{\partial^2 w}{\partial x\partial\theta}\right)+\left(1-l^2\nabla^2\right)\left\{A_{55}\left(\frac{\partial\varphi_x}{\partial x}+\frac{\partial^2 w}{\partial x^2}\right)+A_{66}\left[\frac{1}{R^2}\left(\frac{\partial^2 w}{\partial\theta^2}-\frac{\partial v}{\partial\theta}\right)+\frac{1}{R}\frac{\partial\varphi_\theta}{\partial\theta}\right]\right.\\&\left.-\frac{1}{R}\left[\mathrm{A}_{21}\frac{\partial u}{\partial x}+\mathrm{A}_{22}\frac{1}{R}\left(w+\frac{\partial v}{\partial\theta}\right)\right]\right\}-X_{21}\frac{\partial^2\Psi}{\partial x^2}-\frac{X_{23}}{R}\frac{\partial^2\Psi}{\partial\theta^2}=0\end{aligned} \tag{20c}$$

$$\left(1-l^2\nabla^2\right)\left\{\left(\mathrm{D}_{11}\frac{\partial^2\varphi_x}{\partial x^2}+\mathrm{D}_{12}\frac{1}{R}\frac{\partial^2\varphi_\theta}{\partial x\partial\theta}\right)+\frac{\mathrm{D}_{66}}{R}\left(\frac{\partial^2\varphi_\theta}{\partial x\partial\theta}+\frac{1}{R}\frac{\partial^2\varphi_x}{\partial\theta^2}\right)-A_{55}\left(\varphi_x+\frac{\partial w}{\partial x}\right)\right\}+X_{35}\frac{\partial\Psi}{\partial x}+X_{21}\frac{\partial\Psi}{\partial x}=0 \tag{20d}$$

$$\begin{aligned}&\left(1-l^2\nabla^2\right)\left\{\mathrm{D}_{66}\left(\frac{\partial^2\varphi_\theta}{\partial x^2}+\frac{1}{R}\frac{\partial^2\varphi_x}{\partial x\partial\theta}\right)+\left(\frac{\mathrm{D}_{21}}{R}\frac{\partial^2\varphi_x}{\partial x\partial\theta}+\mathrm{D}_{22}\frac{1}{R^2}\frac{\partial^2\varphi_\theta}{\partial\theta^2}\right)-A_{66}\left[\frac{1}{R}\left(\frac{\partial w}{\partial\theta}-v\right)+\varphi_\theta\right]\right\}\\&+\frac{X_{63}}{R}\frac{\partial\Psi}{\partial\theta}+X_{23}\frac{\partial\Psi}{\partial\theta}=0\end{aligned} \tag{20e}$$

$$\begin{aligned}&X_{21}\left(\frac{\partial\varphi_x}{\partial x}+\frac{\partial^2 w}{\partial x^2}\right)+X_{23}\left[\frac{1}{R}\left(\frac{\partial^2 w}{\partial\theta^2}-\frac{\partial v}{\partial\theta}\right)+\frac{\partial\varphi_\theta}{\partial\theta}\right]+Y_{22}\frac{\partial^2\Psi}{\partial\theta^2}+Y_{11}\frac{\partial^2\Psi}{\partial x^2}+X_{34}\frac{\partial u}{\partial x}+X_{35}\frac{\partial\varphi_x}{\partial x}\\&+X_{63}\frac{1}{R}\left(\frac{\partial v}{\partial\theta}+w\right)+X_{64}\frac{1}{R}\frac{\partial\varphi_\theta}{\partial\theta}-Y_{33}\Psi=0\end{aligned} \tag{20f}$$

in which the axial membrane magnetic and torsional membrane mechanical forces are as [33–35]

$$\text{Magnetic force}: N^0_{xx}=N^{mag}_{xx}=\int_{-h/2}^{h/2}\bar{q}_{31}\frac{2\psi_0}{h}dz \tag{21a}$$

$$\text{Torsional mechanical force}: T=2\pi R^2 N^0_{x\theta} \tag{21b}$$

where T denotes the torsional mechanical critical force, which should be dependent on the radius (Han & Lu, 2003), which determines the torsional stability condition of the SWCNS.

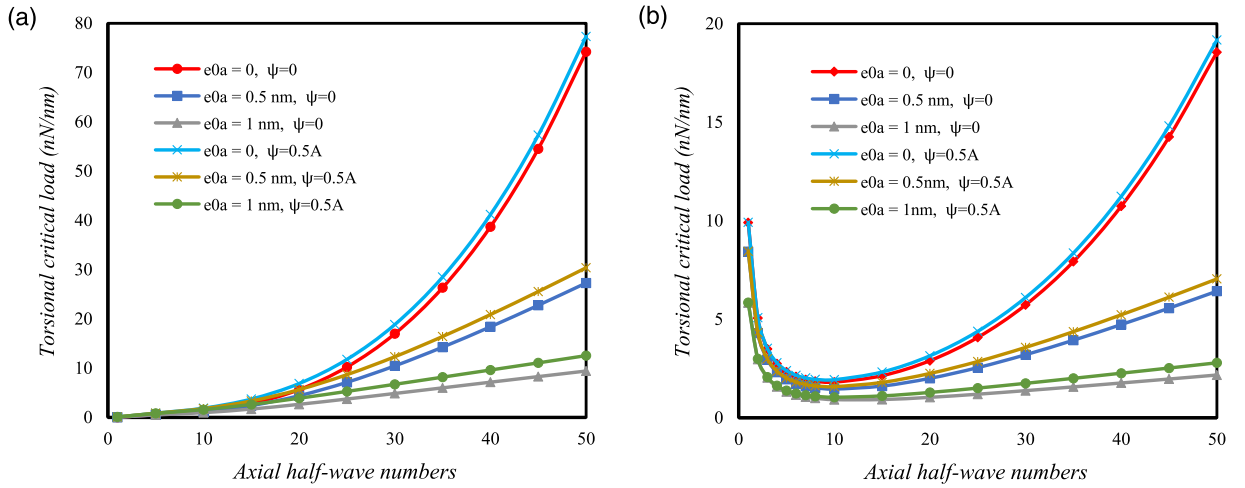

Fig. 2. **(a)** The axial half-wave number vs. stress nonlocality ($l = 0.5$ nm, $n = 1$). **(b)** The axial half-wave number vs. stress nonlocality ($l = 0.5$ nm, $n = 5$).

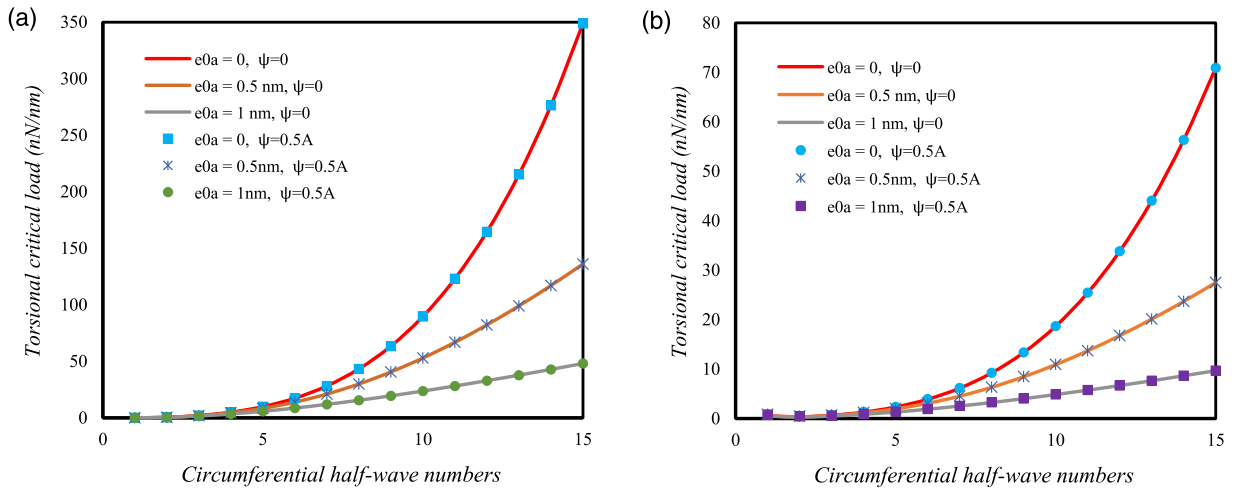

Fig. 3. **(a)** The circumferential half-wave number vs. stress nonlocality ($l = 0.5$ nm, $m = 1$). **(b)** The circumferential half-wave number vs. stress nonlocality ($l = 0.5$ nm, $m = 5$).

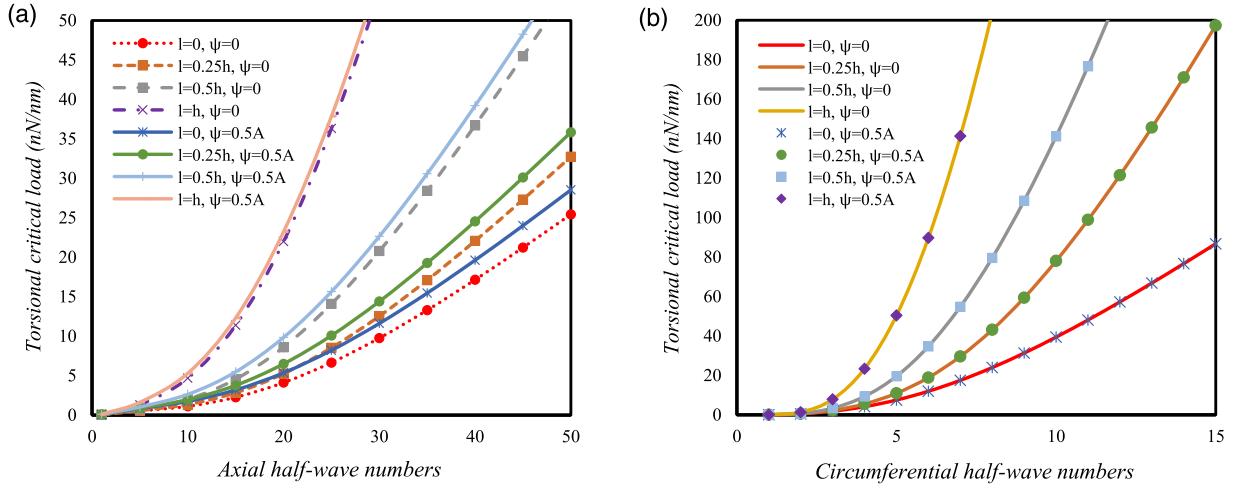

Fig. 4. **(a)** The axial half-wave number vs. strain gradient parameter (e_0a=0.5 nm, $n = 1$). **(b)** The circumferential half-wave number vs. strain gradient parameter (e_0a=0.5 nm, $m = 1$).

3. Solution of equations

In this section, the obtained Eq. (20) is considered to be solved with both ends simply-supported edge conditions. To do this, the below trigonometric displacement functions are utilized (Mehralian et al., 2017).

$$u(x,\theta,t)=\sum_{m=1}^{\infty}\sum_{n=1}^{\infty}U_{mn}\cos\left(\frac{m\pi}{L}x\right)\cos\left(n\theta\right) \tag{22a}$$

$$v(x,\theta,t)=\sum_{m=1}^{\infty}\sum_{n=1}^{\infty}V_{mn}\sin\left(\frac{m\pi}{L}x\right)\sin\left(n\theta\right) \tag{22b}$$

$$w(x,\theta,t)=\sum_{m=1}^{\infty}\sum_{n=1}^{\infty}W_{mn}\sin\left(\frac{m\pi}{L}x\right)cos(n\theta) \tag{22c}$$

$$\varphi_x(x,\theta,t)=\sum_{m=1}^{\infty}\sum_{n=1}^{\infty}\Phi_{xmn}\cos\left(\frac{m\pi}{L}x\right)\cos\left(n\theta\right) \tag{22d}$$

$$\varphi_\theta(x,\theta,t)=\sum_{m=1}^{\infty}\sum_{n=1}^{\infty}\Phi_{\theta mn}\sin\left(\frac{m\pi}{L}x\right)\sin\left(n\theta\right) \tag{22e}$$

$$\Psi(x,\theta,t)=\sum_{m=1}^{\infty}\sum_{n=1}^{\infty}\Theta_{mn}\sin\left(\frac{m\pi}{L}x\right)cos(n\theta) \tag{22f}$$

in which the axial and circumferential half-wave numbers are defined with m and n. By embedding Eq. (22) into Eq. (20), manipulating and also simplifying, we get

$$\begin{bmatrix} K_{11} & K_{12} & K_{13} & 0 & 0 & 0 \\ K_{21} & K_{22} & K_{23} & 0 & K_{25} & K_{26} \\ K_{31} & K_{32} & K_{33} & K_{34} & K_{35} & K_{36} \\ 0 & 0 & K_{43} & K_{44} & K_{45} & K_{46} \\ 0 & K_{52} & K_{53} & K_{54} & K_{55} & K_{56} \\ 0 & K_{62} & K_{63} & K_{64} & K_{65} & K_{66} \end{bmatrix} \begin{Bmatrix} U_{mn} \\ V_{mn} \\ W_{mn} \\ \Phi_{xmn} \\ \Phi_{\theta mn} \\ \Theta_{mn} \end{Bmatrix} = \begin{Bmatrix} 0 \\ 0 \\ 0 \\ 0 \\ 0 \\ 0 \end{Bmatrix} \tag{23}$$

where the matrix K_{ij} is the coefficients one (The elements of the matrix are presented in Appendix A). Setting the determinant of the coefficients matrix to zero gives the characteristic equation of the torsional stability of the SWCNS.

4. Numerical results

4.1. Verification of results

As far as no literature has been reported till now on the torsional buckling of a nano-composite shell inserted in a three-dimensional magnetic field, therefore, the formulation would be reduced into a nano-shell/tube under torsion with removing magnetic effects. On the other hand, in order to compare the results of the torsional buckling of the nano-shell, the molecular dynamics (MD) simulation as Table 1 in which the comparable results are found, is taken into validation (Chowdhurry et al., 2014). As can be observed, outcomes of the FSDT shell model while the size-dependent approach is NSGT, are in good agreement with those of MD. Although the numerical results originated from NSGT completely depend on the correct values of the parameters e_0a and l, these factors should be obligatory obtained in an experiment.

4.2. Parametric study

To proceed with the parametric solution for the nano-composite shell, the properties mentioned in Table 2 are employed.

To make the numerical outcomes, first, the effect of stress nonlocality versus magnetic field by variations in axial half-wave numbers is depicted. To do this, Figure 2a is for $n = 1$ and Figure 2b is drawn for $n = 5$. As it is shown, the increase of axial half-wave numbers tends to increase the torsional capacity. In addition to this, an increase in the magnetic field enlarges the torsional capacity. It is also worthy to note that an increase in axial half-wave numbers remarkably increases the effect of stress nonlocality. This is due to the increase in the distance of curves of the results of various nonlocal parameters. It is also observed that the increase of axial half-wave numbers makes the torsional stability noticeably larger in a local condition than while the stress nonlocality is considered. This is due to the softening effect of the nonlocality. That's why the slope of the results of e_0a=0 in both cases is much steeper. Besides these, it can be conducted that for higher axial half-wave numbers, the impact of magnetic potential in a nonlocal domain is more than a local one. This is because of more gaps between the results of cases e_0a=0.5 nm, ψ=0, with e_0a=0.5 nm, ψ=0.5 A, and also another one. Based on the

Table 1
Results of torsional buckling (nN/nm) of MD for single-walled carbon nanotubes.

SWCNT ($^{*}a = 5, b = 5$)			SWCNT (10, 10)			SWCNT (15, 15)			SWCNT (20, 20)		
d = 0.678 nm			d = 1.356 nm			d = 2.034 nm			d = 2.713 nm		
L/d	MD	Present**	L/d	MD	Present	L/d	MD	Present	L/d	MD	Present
2	16	16	1	43.6	43.6	1	53.3	53.3	1.5	46	46
3.1	11.2	11.2	1.5	30.6	30.6	1.4	43.8	43.8	1.8	42	42
4.2	8.9	8.9	2.1	24.6	24.6	1.6	39.1	39.1	2	39.2	39.2
4.9	8	8	2.4	22.9	22.9	2	35.3	35.3	2.2	38.7	38.7
6	7.2	7.2	3	20.2	20.2	2.4	31	31	2.6	36.8	36.8
7	6.7	6.7	3.5	19.5	19.5	2.7	27.8	27.8	3	31.7	31.7
8.1	6.5	6.5	4.1	18.5	18.5	3	26.7	26.7	3.5	29	29
8.9	6.3	6.3	4.4	16.8	16.8	3.3	24.6	24.6	3.8	28.4	28.4
9.9	6.2	6.2	5	14.8	14.8	4	22.6	22.6	4	27.7	27.7
			6.1	12.5	12.5	4.6	21.8	21.8	4.5	26.3	26.3
			7	11.2	11.2	5	20.9	20.9			
			7.5	10.8	10.8	5.4	20.8	20.8			
			8	10.4	10.4	6	19	19			
			9	9.9	9.9	6.7	16.8	16.8			
			10	9.6	9.6						
			20	8.4	8.4						

* $d(nm) = \frac{2.46}{\pi}\sqrt{a^2 + ab + b^2}$ (Kok & Wong, 2016).
** FSDT shell theory in conjunction with NSGT ($0 < e_0 a \leq 1.5$ nm, $0 < l \leq 8$ nm).

Table 2
Mechanical and magnetic characteristics of Barium Titanate–Cobalt Ferrite nano-composite shell (Gholami & Ansari, 2017; Ghorbanpour Arani et al., 2013; Mehralian et al., 2017; Shojaeefard et al., 2018).

	Elastic properties (GPa)
$BaTiO_3$–$CoFe_2O_4$	C_{11}=C_{22}=226, C_{12}=125, C_{13}= C_{23}=124, C_{33}=216, C_{44}= C_{55}=44.2, C_{66}=50.5 Piezomagnetic quantities ($N/A.m$) q_{15}= q_{24}=275, q_{31}= q_{32}=290.1, q_{33}=349.9 Magnetic quantities ($N.s^2/C^2$) η_{11}= η_{22}=−297e-6, η_{33}=83.5e-6 Sundry quantities h = 4 nm, R = 6 nm, L = 10R, l^{*}=l/h

second figure, it is clear that while the circumferential half-wave number is greater than one, the increase of axial half-wave numbers does not make the increasing effect only for the numerical results of torsional buckling. And the buckling results would be initially decreased and then increased. Plus, there has been found that when the circumferential half-wave number is bigger than one, the effect of stress nonlocality is remarkable even at lower values of the half-waves. But according to the first figure, the effect is not noticeable for the lower values of the half-waves.

To consider the influence of stress nonlocality and magnetic field more deeply, Figure 3a,b as similar as the previous ones are indicated, however by changes in circumferential half-wave numbers. Regarding both presented figures, it can be witnessed that the increase of the circumferential half-wave numbers makes the torsional stability fundamentally further than axial ones. It is noteworthy that the increase of circumferential half-wave numbers even if the axial wave number is chosen as greater than one, leads to a steadily increasing trend for buckling loads. The important point of these two figures, however, can be the fact that for larger circumferential half-wave numbers, there has never been seen any major impact on variations of the magnetic potential.

To clarify the influences of the strain gradient scale parameter, Fig. 4a and b are revealed, respectively. Based on these figures it can be remarked that the increase of the strain gradient parameter leads to decreasing the effect of the magnetic field. This is in light of the distances between results of $l = 0$, ψ=0 and $l = 0$, ψ=0.5A with $l = h$, ψ=0 and $l = h$, ψ=0.5A. In fact, the distance is lower for the second case leads to this conclusion that the increase of torsional buckling loads which resulted from the increase of the magnetic potential is lower in the larger values of the strain gradient parameter. It can be somehow stated that if the material is stiffer, the increase of magnetic potential does not affect outstandingly the stability. On the other hand, as is clear, the increase of the axial half-wave numbers when the strain gradient parameter is chosen as larger, results in a greater impact of the waves on the torsional stability. This means the larger the values of the strain gradient factor, the greater the impact of the axial half-wave numbers.

To study the effect of an increase of magnetic potential on the torsional stability response of the nano-composite shell, the Fig. 5a–c is displayed, respectively. The first two figures are plotted for changes of axial half-wave numbers and the third figure shows the role of changes of circumferential half-wave numbers. For the first figure, the circumferential half-wave is chosen as $n = 1$ and subsequently the $n = 10$ for the second figure. As shown by the first figure, the increase of

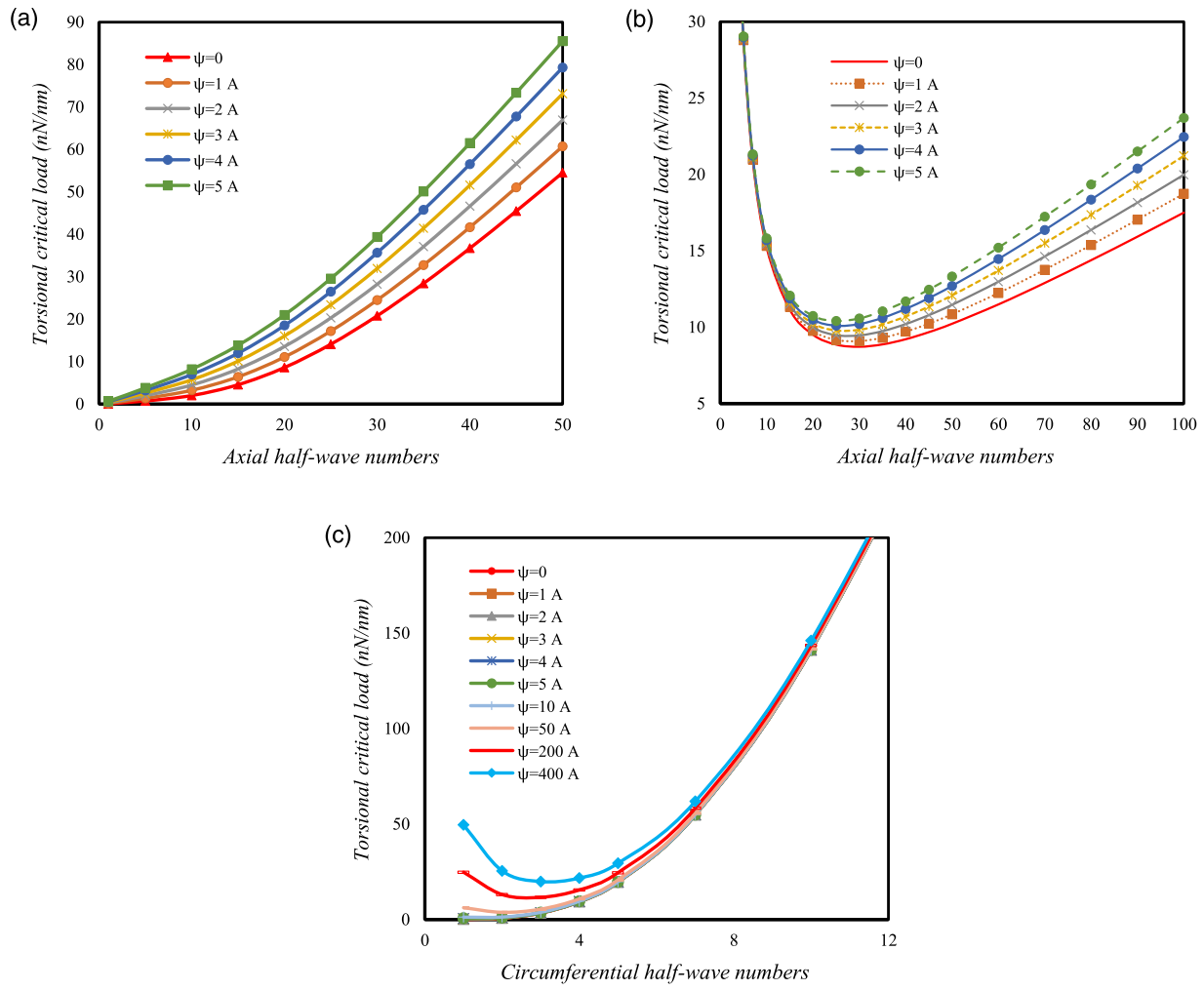

Fig. 5. **(a)** The axial half-wave number vs. magnetic influences (e_0a=0.5 nm, l^*=0.5, $n = 1$). **(b)** The axial half-wave number vs. magnetic influences (e_0a=0.5 nm, l^*=0.5, $n = 10$). **(c)** The circumferential half-wave number vs. magnetic influences (e_0a=0.5 nm, l^*=0.5, $m = 1$).

the magnetic potential increases further the torsional stability by an increase of the axial half-wave numbers. This result is also achieved for the second figure. Additionally, by comparing Figs. 2b and 5b, it is interesting to say that whenever the circumferential half-wave number is selected bigger, the negative slope of curves of results which is related to the lower axial wave numbers, is steeper. On the other side, Fig. 5c illustrates that even powerful and high magnetic environments cannot affect the torsional stability of the nano-composite shell while the circumferential half-wave number is large. Either way, about the effect of the magnetic surrounding on the circumferential wave numbers, it can be said that the strong magnetic field affects the shell's stability if and only if the circumferential half-wave number is small.

In order to consider the effect of a three-dimensional magnetic field versus other magnetic fields, initially, the axial half-wave number is investigated while the magnetic potential is for two cases, weak and powerful magnetic fields which are shown by Fig. 6a and b respectively. From the first figure, as it is vividly seen, when the magnetic field three-dimensionally affected the model, the torsional stability capacity of the shell is lower. But, on the other hand, when the effect is two-dimensional as well as while the transverse effect (B_z=0) is neglected, the highest stability for the nano-shell is predicted. This means that the transverse magnetic effect makes weaker the composite shell under torsional conditions. By comparing the results of three cases of one-dimensional magnetic effect, one can find that on the torsional stability of nano-shells, the transverse magnetic effect (B_z=0), circumferential magnetic effect (B_θ=0) and axial magnetic effect (B_x=0) respectively are making the model weaker under torsion. This can prove that the effect of transverse magnetic is more significant than the others. It is also worth mentioning that when we have a three-dimensional magnetic effect; the stability is further than when there is a two-axis effect by assuming B_x=0. It is also interesting to note that by the increase of the axial half-wave numbers the importance of analysis of magnetic effect in various directions can be demonstrated. In fact, this can be in light of the increase in the distances between the results of various cases in the diagram by the increase of the wave numbers. Moreover, after looking into the second plotted figure, it can be clearly seen that the second diagram also approves the

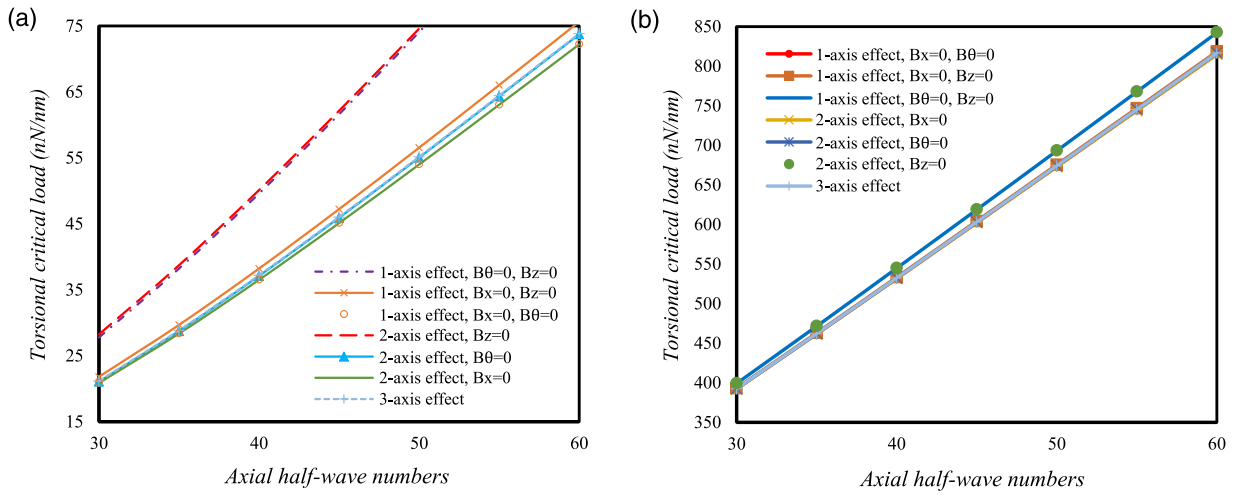

Fig. 6. **(a)** The axial half-wave number vs. three-axis magnetic influences (e_0a=0.5 nm, l^*=0.5, n = 1, ψ=0.1A). **(b)** The axial half-wave number vs. three-axis magnetic influences (e_0a=0.5 nm, l^*=0.5, n = 1, ψ=100A).

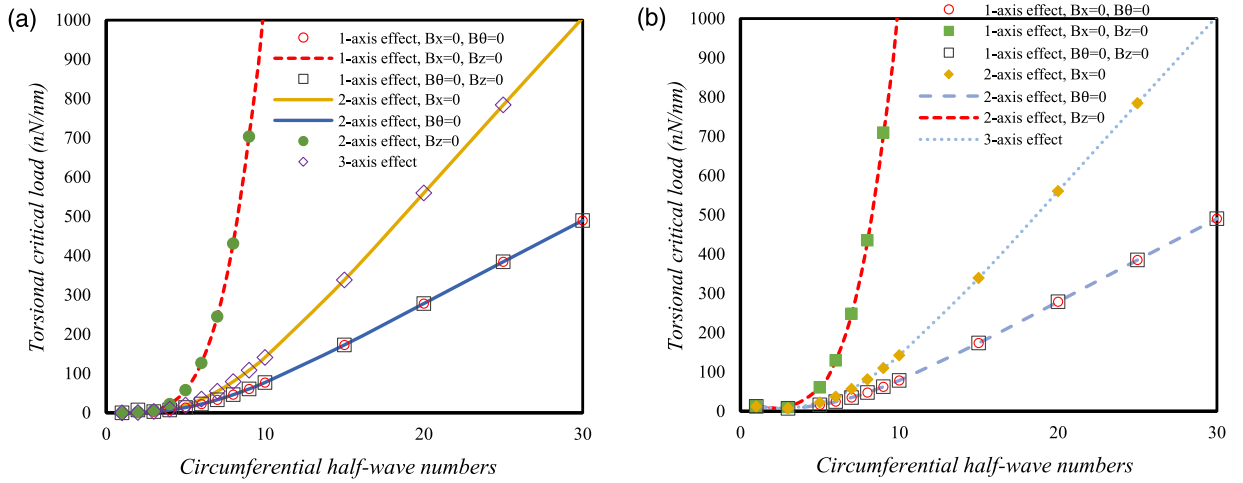

Fig. 7. **(a)** The circumferential half-wave number vs. three-axis magnetic influences (e_0a=0.5 nm, l^*=0.5, m = 1, ψ=0.1A). **(b)** The circumferential half-wave number vs. three-axis magnetic influences (e_0a=0.5 nm, l^*=0.5, m = 1, ψ=100A).

significance of the transverse magnetic effect in a magneto-elastic analysis. The analysis of the high magnetic environment which is appeared by the second figure presents that in a high potential magnetic field, the effect of direction for magnetic potential is lesser. To conclude, these two figures confirmed that even in a nanoscale the direction of magnetic influences is very important.

Fig. 7a and b respectively exhibit the influence of an increase of the circumferential half-wave number under different cases of the magnetic field, first, in a weak magnetic condition and second for a high magnetic condition. First off, in comparison of these two figures with the Fig. 6a and b, one can find that the increase of the circumferential half-wave numbers increases dramatically the importance of the different magnetic fields. In other words, whatever the circumferential wave numbers increased, the results in the figures have become far from each other by a very steep slope. Consequently, in very large circumferential wave numbers, the direction of the magnetic field is seriously important. Furthermore, as shown in the figures, for lower circumferential half-wave numbers, the directions of the magnetic field cannot be considerable.

5. Conclusions

This paper performed a study on the torsional resistance of the nano-composite shell under a three-dimensional magnetic field based on the first-order shear deformation shell approach in combining with the nonlocal theory of strain gradient. In order to take the numerical findings, an analytical approach was used. After validation of numerical outcomes, the role of key parameters was investigated on the torsional behavior of the shell. According to the remarkable findings, some notes are summarized as below

- In a three-dimensional magnetic analysis of the nano-composite shell, the most important magnetic effect can be for the transverse effect.
- While the larger amounts of circumferential half-wave numbers are considered, it is very important to study the three-dimensional magnetic field.
- The influence of the magnetic environment is more remarkable for the larger axial half-wave numbers.
- The larger amounts of the strain gradient parameter, the smaller the effect of magnetic potential.
- The higher values of the axial half-wave number, the higher the impact of the magnetic potential in a nonlocal domain.

Acknowledgements

The second and third authors acknowledge the support by grant 14.Z50.31.0036 awarded to R. E. Alekseev Nizhny Novgorod Technical University by Department of Education and Science of the Russian Federation.

Appendix A

$$K_{11} = -\mathrm{A}_{11}\left(\frac{m\pi}{L}\right)^2 - \frac{\mathrm{A}_{44}n^2}{R^2}$$
$$K_{12} = \frac{\mathrm{A}_{12}}{R}\frac{m\pi\, n}{L} + \frac{\mathrm{A}_{44}}{R}\frac{m\pi\, n}{L}$$
$$K_{13} = \frac{\mathrm{A}_{12}}{R}\frac{m\pi}{L}$$

$$K_{21} = \frac{\mathrm{A}_{44}}{R}\frac{m\pi\, n}{L} + \frac{\mathrm{A}_{21}}{R}\frac{m\pi\, n}{L} + \frac{\mathrm{A}_{44}l^2 n}{R}\left(\frac{m\pi}{L}\right)^3 + \frac{\mathrm{A}_{21}l^2 n}{R}\left(\frac{m\pi}{L}\right)^3 + \frac{\mathrm{A}_{44}l^2 n^3}{R^3}\frac{m\pi}{L} + \frac{\mathrm{A}_{21}l^2 n^3}{R^3}\frac{m\pi}{L}$$
$$K_{22} = -\mathrm{A}_{44}\left(\frac{m\pi}{L}\right)^2 - \frac{\mathrm{A}_{22}n^2}{R^2} - \frac{A_{66}}{R^2} - \mathrm{A}_{44}l^2\left(\frac{m\pi}{L}\right)^4 - \frac{\mathrm{A}_{22}l^2n^2}{R^2}\left(\frac{m\pi}{L}\right)^2 - \frac{l^2A_{66}}{R^2}\left(\frac{m\pi}{L}\right)^2$$
$$- \frac{\mathrm{A}_{44}l^2n^2}{R^2}\left(\frac{m\pi}{L}\right)^2 - \frac{\mathrm{A}_{22}l^2n^4}{R^4} - \frac{l^2A_{66}n^2}{R^4}$$
$$K_{23} = -\frac{\mathrm{A}_{22}n}{R^2} - \frac{l^2\mathrm{A}_{22}n}{R^2}\left(\frac{m\pi}{L}\right)^2 - \frac{l^2\mathrm{A}_{22}n^3}{R^4} - \frac{A_{66}n}{R^2} - \frac{l^2A_{66}n}{R^2}\left(\frac{m\pi}{L}\right)^2 - \frac{l^2A_{66}n^3}{R^4}$$
$$K_{25} = \frac{A_{66}}{R} + \frac{l^2A_{66}}{R}\left(\frac{m\pi}{L}\right)^2 + \frac{l^2A_{66}n^2}{R^3}$$
$$K_{26} = \frac{X_{23}n}{R}$$

$$K_{31} = \frac{\mathrm{A}_{21}}{R}\frac{m\pi}{L} + \frac{l^2\mathrm{A}_{21}}{R}\left(\frac{m\pi}{L}\right)^3 + \frac{l^2\mathrm{A}_{21}n^2}{R^3}\frac{m\pi}{L}$$
$$K_{32} = -\frac{A_{66}n}{R^2} - \frac{A_{66}l^2n}{R^2}\left(\frac{m\pi}{L}\right)^2 - \frac{A_{66}l^2n^3}{R^4} - \frac{\mathrm{A}_{22}n}{R^2} - \frac{\mathrm{A}_{22}l^2n}{R^2}\left(\frac{m\pi}{L}\right)^2 - \frac{\mathrm{A}_{22}l^2n^3}{R^4}$$
$$K_{33} = -N^0_{xx}\left(\frac{m\pi}{L}\right)^2 - \mu N^0_{xx}\left(\frac{m\pi}{L}\right)^4 - \frac{\mu n^2}{R^2}N^0_{xx}\left(\frac{m\pi}{L}\right)^2 - \frac{2}{R}N^0_{x\theta}\frac{m\pi\, n}{L} - \frac{2\mu n}{R}N^0_{x\theta}\left(\frac{m\pi}{L}\right)^3$$
$$- \frac{2\mu n^3}{R^3}N^0_{x\theta}\frac{m\pi}{L} - A_{55}\left(\frac{m\pi}{L}\right)^2 - \frac{A_{66}n^2}{R^2} - A_{55}l^2\left(\frac{m\pi}{L}\right)^4 - \frac{A_{66}l^2n^2}{R^2}\left(\frac{m\pi}{L}\right)^2 - \frac{A_{55}l^2n^2}{R^2}\left(\frac{m\pi}{L}\right)^2$$
$$- \frac{A_{66}l^2n^4}{R^4} - \frac{\mathrm{A}_{22}}{R^2} - \frac{\mathrm{A}_{22}l^2}{R^2}\left(\frac{m\pi}{L}\right)^2 - \frac{\mathrm{A}_{22}l^2n^2}{R^4}$$
$$K_{34} = -A_{55}\frac{m\pi}{L} - A_{55}l^2\left(\frac{m\pi}{L}\right)^3 - \frac{A_{55}l^2n^2}{R^2}\frac{m\pi}{L}$$
$$K_{35} = \frac{A_{66}n}{R} + \frac{A_{66}l^2n}{R}\left(\frac{m\pi}{L}\right)^2 + \frac{A_{66}l^2n^3}{R^3}$$
$$K_{36} = X_{21}\left(\frac{m\pi}{L}\right)^2 + \frac{X_{23}n^2}{R}$$

$$\mathrm{K}_{43} = -A_{55}\frac{m\pi}{L}$$

$$K_{44} = -D_{11}\left(\frac{m\pi}{L}\right)^2 - \frac{D_{66}n^2}{R^2} - A_{55}$$
$$K_{45} = \frac{D_{12}n}{R}\frac{m\pi}{L} + \frac{D_{66}n}{R}\frac{m\pi}{L}$$
$$K_{46} = X_{35}\frac{m\pi}{L} + X_{21}\frac{m\pi}{L}$$

$$K_{52} = \frac{A_{66}}{R} + \frac{A_{66}l^2}{R}\left(\frac{m\pi}{L}\right)^2 + \frac{A_{66}l^2n^2}{R^3}$$
$$K_{53} = \frac{A_{66}n}{R} + \frac{A_{66}l^2n}{R}\left(\frac{m\pi}{L}\right)^2 + \frac{A_{66}l^2n^3}{R^3}$$
$$K_{54} = \frac{D_{66}n}{R}\frac{m\pi}{L} + \frac{D_{21}n}{R}\frac{m\pi}{L} + \frac{l^2D_{66}n}{R}\left(\frac{m\pi}{L}\right)^3 + \frac{l^2D_{21}n}{R}\left(\frac{m\pi}{L}\right)^3 + \frac{l^2D_{66}n^3}{R^3}\frac{m\pi}{L} + \frac{l^2D_{21}n^3}{R^3}\frac{m\pi}{L}$$
$$K_{55} = -D_{66}\left(\frac{m\pi}{L}\right)^2 - \frac{D_{22}n^2}{R^2} - A_{66} - l^2D_{66}\left(\frac{m\pi}{L}\right)^4 - \frac{l^2D_{22}n^2}{R^2}\left(\frac{m\pi}{L}\right)^2 - A_{66}l^2\left(\frac{m\pi}{L}\right)^2 - \frac{l^2D_{66}n^2}{R^2}\left(\frac{m\pi}{L}\right)^2 - \frac{l^2D_{22}n^4}{R^4} - \frac{A_{66}l^2n^2}{R^2}$$
$$K_{56} = -\frac{X_{63}n}{R} - X_{23}n$$

$$K_{61} = -X_{34}\frac{m\pi}{L}$$
$$K_{62} = \frac{X_{63}n}{R} - \frac{X_{23}n}{R}$$
$$K_{63} = -X_{21}\left(\frac{m\pi}{L}\right)^2 - \frac{X_{23}n^2}{R} + \frac{X_{63}}{R}$$
$$K_{64} = -X_{21}\frac{m\pi}{L} - X_{35}\frac{m\pi}{L}$$
$$K_{65} = X_{23}n + \frac{X_{64}}{R}n$$
$$K_{66} = -Y_{22}n^2 - Y_{11}\left(\frac{m\pi}{L}\right)^2 - Y_{33}$$

References

Akbarzadeh Khorshidi, M. (2018). The material length scale parameter used in couple stress theories is not a material constant. *International Journal of Engineering Science, 133*, 15–25.

Akgöz, B., & Civalek, Ö. (2012). Free vibration analysis for single-layered graphene sheets in an elastic matrix via modified couple stress theory. *Materials & Design, 42*, 164–171.

Arefi, M., Kiani, M., & Rabczuk, T. (2019). Application of nonlocal strain gradient theory to size dependent bending analysis of a sandwich porous nanoplate integrated with piezomagnetic face-sheets. *Composites Part B: Engineering, 168*, 320–333.

Chowdhurry, A. N. R., Wang, C. M., & Koh, S. J. A. (2014). Continuum shell model for buckling of armchair carbon nanotubes under compression or torsion. *International Journal of Applied Mechanics, 6*(1), 1450006.

Elimelech, M., Gregory, J., Jia, X., & Williams, R. A. (1995). Chapter 15 - Application of simulation techniques to colloidal dispersion systems. *Particle Deposition & Aggregation, Measurement, Modelling and Simulation*, 402–425. doi:10.1016/B978-075067024-1/50015-7.

Eringen, A. C. (1983). On differential equations of nonlocal elasticity and solutions of screw dislocation and surface waves. *Journal of Applied Physics, 54*(9), 4703–4710.

Farajpour, A., Ghayesh, M. H., & Farokhi, H. (2019). Nonlocal nonlinear mechanics of imperfect carbon nanotubes. *International Journal of Engineering Science, 142*, 201–215.

Gholami, R., & Ansari, R. (2017). A unified nonlocal nonlinear higher-order shear deformable plate model for postbuckling analysis of piezoelectric-piezomagnetic rectangular nanoplates with various edge supports. *Composite Structures, 166*, 202–218.

Gholami, R., Darvizeh, A., Ansari, R., & Sadeghi, F. (2016). Vibration and buckling of first-order shear deformable circular cylindrical micro-/nano-shells based on Mindlin's strain gradient elasticity theory. *European Journal of Mechanics - A/Solids, 58*, 76–88.

Ghorbanpour Arani, A., Abdollahian, M., Kolahchi, R., & Rahmati, A. H. (2013). Electro-thermo-torsional buckling of an embedded armchair DWBNNT using nonlocal shear deformable shell model. *Composites: Part B, 51*, 291–299.

Han, Q., & Lu, G. (2003). Torsional buckling of a double-walled carbon nanotube embedded in an elastic medium. *European Journal of Mechanics A/Solids, 22*(6), 875–883.

Hao, M. J., Guo, X. M., & Wang, Q. (2010). Small-scale effect on torsional buckling of multi-walled carbon nanotubes. *European Journal of Mechanics A/Solids, 29*(1), 49–55.

Jeong, B.-W., Lim, J.-K., & Sinnott, S. B. (2007). Elastic torsional responses of carbon nanotube systems. *Journal of Applied Physics, 101*, 084309.

Karami, B., Shahsavari, D., & Janghorban, M. (2019). On the dynamics of porous doubly-curved nanoshells. *International Journal of Engineering Science, 143*, 39–55.

Khademolhosseini, F., Rajapakse, R. K. N. D., & Nojeh, A. (2010). Torsional buckling of carbon nanotubes based on nonlocal elasticity shell models. *Computational Materials Science, 48*(4), 736–742.

Kok, Z. K. J., & Wong, C. H. (2016). Molecular dynamics simulation studies of mechanical properties of different carbon nanotube systems. *Molecular Simulation, 42*(15), 1274–1280.

Lim, C. W., Zhang, H., & Reddy, J. N. (2015). A higher-order nonlocal elasticity and strain gradient theory and its applications in wave propagation. *Journal of the Mechanics and Physics of Solids, 78*, 298–313.
Lu, Y. J., & Wang, X. (2006). Combined torsional buckling of multi-walled carbon nanotubes. *Journal of Physics D: Applied Physics, 39*(15), 3380–3387.
Lurie, S., & Solyaev, Y. (2019a). On the formulation of elastic and electroelastic gradient beam theories. *Continuum Mechanics and Thermodynamics, 31*(6), 1601–1613.
Lurie, S., & Solyaev, Y. (2019b). Anti-plane inclusion problem in the second gradient electroelasticity theory. *International Journal of Engineering Science, 144*, 103129.
Malikan, M. (2017). Electro-mechanical shear buckling of piezoelectric nanoplate using modified couple stress theory based on simplified first order shear deformation theory. *Applied Mathematical Modelling, 48*, 196–207.
Malikan, M., Dimitri, R., & Tornabene, F. (2019). Transient response of oscillated carbon nanotubes with an internal and external damping. *Composites Part B: Engineering, 158*, 198–205.
Malikan, M., & Nguyen, V. B. (2018). Buckling analysis of piezo-magnetoelectric nanoplates in hygrothermal environment based on a novel one variable plate theory combining with higher-order nonlocal strain gradient theory. *Physica E: Low-dimensional Systems and Nanostructures, 102*, 8–28.
Mehralian, F., Tadi Beni, Y., & Karimi Zeverdejani, M. (2017). Nonlocal strain gradient theory calibration using molecular dynamics simulation based on small scale vibration of nanotubes. *Physica B: Physics of Condensed Matter, 514*, 61–69.
Mikhasev, G., & Nobili, A. (2019). On the solution of the purely nonlocal theory of beam elasticity as a limiting case of the two-phase theory. *International Journal of Solids and Structures*. doi:10.1016/j.ijsolstr.2019.10.022.
Mikhasev, G. I., Eremeyev, V. A., Wilde, K., & Maevskaya, S. S. (2019). Assessment of dynamic characteristics of thin cylindrical sandwich panels with magnetorheological core. *Journal of Intelligent Material Systems and Structures, 30*(18–19), 2748–2769.
Natsuki, T., Tsuchiya, T., Ni, Q. Q., & Endo, M. (2010). Torsional elastic instability of double-walled carbon nanotubes. *Carbon, 48*(15), 4362–4368.
Parvaneh, V., Shariati, M., Torabi, H., Masood, A., & Sabeti, M. (2012). Torsional buckling behavior of SWCNTs using a molecular structural mechanics approach considering vacancy defects. *Fullerenes, Nanotubes and Carbon Nanostructures, 20*(8), 709–720.
Reddy, J. N. (2007). Nonlocal theories for bending, buckling and vibration of beams. International Journal of Engineering Science, *45*(2–8), 288–307.
Sahmani, S., & Aghdam, M. M. (2017). Nonlinear instability of axially loaded functionally graded multilayer graphene platelet-reinforced nanoshells based on nonlocal strain gradient elasticity theory. *International Journal of Mechanical Sciences, 131–132*, 95–106.
Sahmani, S., & Aghdam, M. M. (2018). Nonlocal strain gradient shell model for axial buckling and postbuckling analysis of magneto-electro-elastic composite nanoshells. *Composites Part B: Engineering, 132*, 258–274.
She, G.-L., Yuan, F.-G., Karami, B., Ren, Y.-R., & Xiao, W.-S. (2019). On nonlinear bending behavior of FG porous curved nanotubes. *International Journal of Engineering Science, 135*, 58–74.
Shen, H.-S., & Zhang, C.-L. (2010). Torsional buckling and postbuckling of double-walled carbon nanotubes by nonlocal shear deformable shell model. *Composite Structures, 92*(5), 1073–1084.
Shojaeefard, M. H., Mahinzare, M., Safarpour, H., Saeidi Googarchin, H., & Ghadiri, M. (2018). Free vibration of an ultra-fast-rotating-induced cylindrical nano-shell resting on a Winkler foundation under thermo-electro-magneto-elastic condition. *Applied Mathematical Modelling, 61*, 255–279.
Solyaev, Y., & Lurie, S. (2019). Pure bending of a piezoelectric layer in second gradient electroelasticity theory. *Acta Mechanica, 230*(12), 4197–4211.
Solyaev, Y., Lurie, S., Koshurina, A., Dobryanskiy, V., & Kachanov, M. (2019). On a combined thermal/mechanical performance of a foam-filled sandwich panels. *International Journal of Engineering Science, 134*, 66–76.
Song, H.-Y., & Zha, X.-W. (2011). Molecular dynamics study of effects of nickel coating on torsional behavior of single-walled carbon nanotube. *Physica B, 406*(4), 992–995.
Wang, Q., Quek, S. T., & Varadan, V. K. (2007). Torsional buckling of carbon nanotubes. *Physics Letters A, 367*(1–2), 135–139.
Wang, X., Yang, H. K., & Dong, K. (2005). Torsional buckling of multi-walled carbon nanotubes. *Materials Science and Engineering A, 404*(1–2), 314–322.
Xiaohu, Y., Yugang, S., & Hanzhou, L. (2013). Combined torsional buckling of carbon nanotubes subjected to thermo-electro-mechanical loadings with consideration of scale effect. *Key Engineering Materials, 562-565*, 744–749.
Yang, H. K., & Wang, X. (2007). Torsional buckling of multi-wall carbon nanotubes embedded in an elastic medium. *Composite Structures, 77*(2), 182–192.
Zhang, C.-L., & Shen, H.-S. (2006). Buckling and postbuckling analysis of single-walled carbon nanotubes in thermal environments via molecular dynamics simulation. *Carbon, 44*(13), 2608–2616.
Zhang, Q. W., & Li, B. (2015). Torsional behavior of single-walled carbon nanotubes. *Carbon, 94*, 826–835.
Zhang, Y. Y., & Wang, C. M. (2008). Torsional responses of double-walled carbon nanotubes via molecular dynamics simulations. *Journal of Physics: Condensed Matter, 20*(45), 455214.